Ab initio supercell calculations on nitrogen-vacancy center in diamond: Electronic structure and hyperfine tensors

Adam Gali,[1,2] Maria Fyta,[2] and Efthimios Kaxiras[2]
[1]*Department of Atomic Physics, Budapest University of Technology and Economics, Budafoki út 8, H-1111 Budapest, Hungary*
[2]*Department of Physics and School of Engineering and Applied Sciences, Harvard University, Cambridge, Massachusetts 02138, USA*
(Received 5 March 2008; revised manuscript received 21 March 2008; published 15 April 2008)

The nitrogen-vacancy center in diamond is a promising candidate for realizing the spin qubits concept in quantum information. Even though this defect has been known for a long time, its electronic structure and other properties have not yet been explored in detail. We study the properties of the nitrogen-vacancy center in diamond through density functional theory within the local spin density approximation by using supercell calculations. While this theory is strictly applicable for ground state properties, we are able to give an estimate for the energy sequence of the excited states of this defect. We also calculate the hyperfine tensors in the ground state. The results clearly show that (i) the spin density and the appropriate hyperfine constants are spread along a plane and unevenly distributed around the core of the defect and (ii) the measurable hyperfine constants can be found within about 7 Å from the vacancy site. These results have important implications on the decoherence of the electron spin which is crucial in realizing the spin qubits in diamond.

DOI: 10.1103/PhysRevB.77.155206 PACS number(s): 71.15.Mb

I. INTRODUCTION

The nitrogen-vacancy (NV) center in diamond has attracted much attention in recent years because it has been shown to give rise to a single optically active level within the diamond band gap,[1,2] and as such provides an interesting candidate for a qubit for quantum computing applications.[3–8] Besides providing a single photon source for quantum cryptography,[9,10] the NV center is also a promising candidate as an optically coupled quantum register for scalable quantum information processing, such as quantum communication[11] and distributed quantum computation.[12] In addition, it has been recently demonstrated that proximal nuclear spins can be coherently controlled via hyperfine interaction[13] and used as a basis for quantum memory with an extremely long coherence time.[14] Therefore, knowing the electron-nucleus hyperfine interaction and its position dependence is essential to analyze and optimize coherent control of proximal nuclear spins.[15]

Experimentally, the hyperfine constants of the closest atoms near the vacancy are known from electron paramagnetic resonance (EPR) and electron-nuclear double resonance (ENDOR) studies.[16,17] The hyperfine interaction between ^{13}C isotopes farther from the vacancy contributes to the coherent electron-nuclear spin states in the measurements.[13,14] *Ab initio* supercell calculations can be a very useful tool for determining the hyperfine tensors of a defect. For instance, such calculations have been used to identify the basic vacancy defects in silicon carbide by comparing the measured and calculated hyperfine constants.[18–21] In the present paper, we focus on the calculation of the full hyperfine tensor of the NV center in diamond, which is of very high importance for qubit applications. Previous theoretical work has reported a calculation of the hyperfine constants of the NV center in a small 64-atom supercell,[22] but that work determined only the Fermi-contact term rather than the full hyperfine tensor. We will show in the Results and Discussion section that the conclusions based on that earlier analysis were adversely affected by the small unit cell size. The larger supercell of 512 atoms employed here does not suffer from this limitation and provides a realistic picture for the defect properties, which are in excellent agreement with experimental measurements.

The rest of this paper is organized as follows: Section II gives a general discussion of the electronic states of the NV center based on a single-particle picture and the many-body states that can be constructed from this basis. Section III describes the method of the first-principles calculations we performed. Section IV presents and discusses our results concerning the atomic and electronic structure of the defect, as obtained from the *ab initio* calculations. In Sec. V, we present a detailed discussion of the calculated hyperfine interactions. Finally, we give our conclusions on the nature of this defect in Sec. VI.

II. ELECTRONIC STATES OF THE NITROGEN-VACANCY CENTER IN DIAMOND

The electronic structure of the NV center in diamond has been discussed in detail in a recent paper;[23] we briefly review the main points here. The NV center was found many years ago in diamond.[24] The concentration of NV centers can be enhanced in N-contaminated diamond by irradiation and annealing.[24,25] The model of the NV center consists of a substitutional nitrogen atom adjacent to a vacancy in diamond.[16,24–26] The NV center has a strong optical transition with a zero phonon line (ZPL) at 1.945 eV (637 nm) accompanied by a vibronic band at higher energy in absorption and lower energy in emission. Detailed analysis of the ZPL revealed that the center has trigonal C_{3v} symmetry.[25] Later, an optically induced EPR center was found in diamond which correlated with the NV center.[16] The EPR center showed trigonal symmetry with a spin polarized triplet state ($S=1$). Since the nitrogen atom has five valence electrons and the $S=1$ state implies an even number of electrons, the NV defect must be charged in the EPR measurement. It was as-

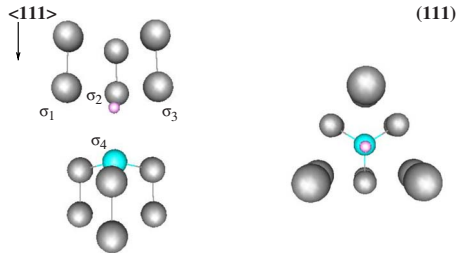

FIG. 1. (Color online) The NV center viewed in perspective (left) and along the ⟨111⟩ direction (right); this direction is the C_3 symmetry axis of the C_{3v} symmetry group of the defect. The vacant site is indicated by a small pink circle and the neighboring C and N atoms by gray and cyan balls, respectively. The first neighbor atoms around the vacant site have sp^3 dangling bonds pointing toward the vacant site, which are labeled σ_i ($i=1,4$), as in the scheme used in the group theory analysis.

sumed that the NV defect is negatively charged and the extra electron may be donated from isolated substitutional nitrogen defects.[16] In a recent measurement, the coupling between the NV center and the nitrogen substitutional has been indeed detected.[27] Loubser and van Wyk[16] measured the NV EPR signal just under the optical excitation, based on which they proposed that the spin polarization arises from a singlet electronic system with intersystem crossing to a spin level of a metastable triplet. Redman *et al.*[28] detected the NV center in the dark even at 100 K by EPR, from which they concluded that the $S=1$ state is the ground state of the NV center. Hole burning,[29] optically detected magnetic resonance,[30] and Raman heterodyne measurements[31] also showed that the $S=1$ state is the ground state of the NV center.

A group theory analysis based on a single-particle picture can be very useful in understanding the nature of the defect states and the possible optical transitions between them. While the number of electrons in the NV center has been disputed in the literature,[32,33] a previous *ab initio* calculation clearly supported the negatively charged NV defect,[34] as was originally proposed by Loubser and van Wyk.[16] We will also show in the Results and Discussion section that the NV center should be negatively charged.

In the NV defect, three carbon atoms have sp^3 dangling bonds near the vacancy and three back bonds each pointing to the lattice, while the nitrogen atom has also three back bonds and one dangling bond pointing to the vacant site. Since nitrogen has five valence electrons the negatively charged NV defect has altogether six electrons around the vacant site. The structure of the NV defect, including the definition of the symmetry ⟨111⟩ axis, is depicted in Fig. 1.

The group theory analysis of the six electron model has been previously worked out for this defect.[35] We summarize the results using our notation and conventions: Since it is known that the carbon and nitrogen atoms relax outward from the vacancy,[22,34] we assume that the overlap between the dangling bonds (σ_{1-4}) is negligible, that is, $\sigma_i\sigma_j=\delta_{ij}$. σ_{1-4} are transformed under the operation of the C_{3v} point group, forming the following orthonormal states:

$$a_1(1):\phi_1 = \sqrt{1-\alpha^2}\sigma_4 - \frac{\alpha}{\sqrt{3}}(\sigma_1+\sigma_2+\sigma_3),$$

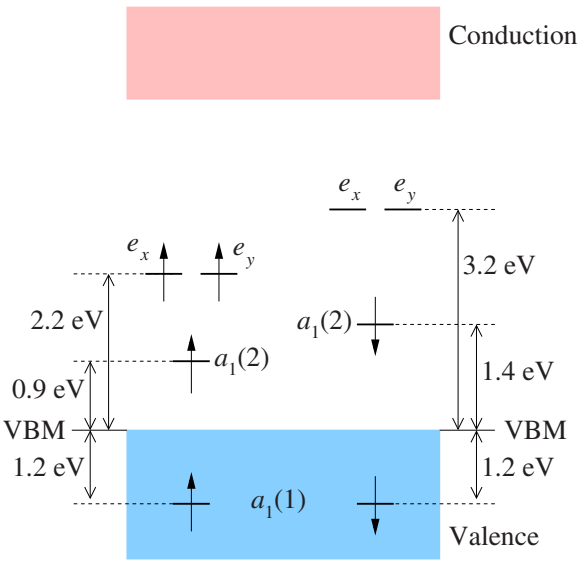

FIG. 2. (Color online) The calculated spin-resolved single-electron levels with respect to the valence band maximum (VBM) in the ground state of the NV defect. Valence and conduction bands of the host crystal are shown as blue and pink shaded regions, respectively. The levels are labeled as in Eq. (1) and their occupation is given for a negatively charged defect (a total of six electrons).

$$a_1(2):\phi_2 = \alpha\sigma_4 + \sqrt{\frac{1-\alpha^2}{3}}(\sigma_1+\sigma_2+\sigma_3),$$

$$e_x:\phi_3 = \frac{1}{\sqrt{6}}(2\sigma_1-\sigma_2-\sigma_3),$$

$$e_y:\phi_4 = \frac{1}{\sqrt{2}}(\sigma_2-\sigma_3), \quad (1)$$

where $0\leqslant\alpha\leqslant 1$ is a parameter that determines the extent to which the nitrogen dangling bond is mixed in the ϕ_1 and ϕ_2 defect states. There are two fully symmetric one-electron states (a_1) and one doubly degenerate e state, with a total occupation of six electrons. We note here that the dangling bond of nitrogen is *not* mixed in the e state but only in the a_1 states. It was found by Goss *et al.*[34] by using *ab initio* molecular cluster calculations that the two a_1 states are lower in energy than the e state. As a consequence, four electrons occupy the a_1 states and two electrons remain for the e state. Our calculated one-electron levels obtained by *ab initio* supercell calculations are shown in Fig. 2. As can be seen from this analysis, the natural choice is to put the two remaining electrons in the e level forming an $S=1$ state (by analogy to Hund's rule for the p orbitals of the isolated group IV elements in the Periodic Table).

In the C_{3v} point group, the total wave function has $^3A_2$ symmetry with $S=1$. In our special case, we choose $M_S=1$, so both electrons are spin-up electrons in the e level. The C_{3v} symmetry can also be maintained by other occupations of the states. Putting two electrons into four possible quantum states of the degenerate e level, we end up with six possible

TABLE I. The electronic configurations and the possible total wave functions with C_{3v} symmetry. For simplicity, we abbreviate $\sigma_2 \rightarrow 2$, etc., in the last column. The overbar in a wave function means spin-down electrons, while the rest are spin-up electrons. We assume that $a_1(1):\sigma_1$ is fully occupied. Hence, here we do not show that part of the wave function. In the second and third columns, we give the symmetry of the total wave function (Γ) and its spin projection (M_S), respectively. In the case of doubly degenerate representations (E states), we designate which transforms as x or y in the last column.

Configuration	Γ	M_S	(x,y)	Wave function
$a_1^2(2)e^2$	$^3A_2$	1		$\|2\bar{2}34\rangle$
		0		$\frac{1}{\sqrt{2}}[\|2\bar{2}3\bar{4}\rangle+\|2\bar{2}\bar{3}4\rangle]$
		−1		$\|2\bar{2}\bar{3}\bar{4}\rangle$
	$^1A_1$	0		$\frac{1}{\sqrt{2}}[\|2\bar{2}3\bar{3}\rangle+\|2\bar{2}4\bar{4}\rangle]$
	^1E	0	x	$\frac{1}{\sqrt{2}}[\|2\bar{2}3\bar{3}\rangle-\|2\bar{2}4\bar{4}\rangle]$
			y	$\frac{1}{\sqrt{2}}[\|2\bar{2}3\bar{4}\rangle-\|2\bar{2}\bar{3}4\rangle]$
$a_1^1(2)e^3$	^3E	1	x	$\|234\bar{4}\rangle$
			y	$\|23\bar{3}4\rangle$
		0	x	$\frac{1}{\sqrt{2}}[\|\bar{2}34\bar{4}\rangle+\|2\bar{3}4\bar{4}\rangle]$
			y	$\frac{1}{\sqrt{2}}[\|\bar{2}3\bar{3}4\rangle+\|23\bar{3}\bar{4}\rangle]$
		−1	x	$\|\bar{2}\bar{3}44\rangle$
			y	$\|\bar{2}3\bar{3}\bar{4}\rangle$
	^1E	0	x	$\frac{1}{\sqrt{2}}[\|\bar{2}34\bar{4}\rangle-\|2\bar{3}4\bar{4}\rangle]$
			y	$\frac{1}{\sqrt{2}}[\|\bar{2}3\bar{3}4\rangle-\|23\bar{3}\bar{4}\rangle]$
$a_1^0(2)e^4$	$^1A_1$	0		$\|3\bar{3}4\bar{4}\rangle$

multiplets (including the degeneracy): $^3A_2$, $^1A_1$, and ^1E. By taking $^3A_2$ to be the ground state of the defect (as experiments indicate), there is no allowed optical transition to first order since the spin state cannot be changed in a phonon line (PL) process. The ϕ_1 level is relatively deep in the valence band, so to a good approximation, we can assume that it does not contribute to the excitation process. However, the ϕ_2 level in the gap is not very far from the e level. If one electron is excited from ϕ_2 into the e level (ϕ_3 or ϕ_4), then either a ^3E or a ^1E multiplet is obtained. If both electrons are excited from ϕ_2 to ϕ_3 and ϕ_4, then a fully symmetric $^1A_1$ state is obtained. The only allowed transition is $^3A_2 \rightarrow {}^3E$ to first order. The electronic configurations of these states are explained in Table I. Most of these states were discussed in Ref. 35.

The $M_S = \pm 1$ triplet states can be described by a single Slater determinant. However, the singlet states (except for the last $^1A_1$ state) can be described by a linear combination of two Slater determinants. The two singlet single-Slater-determinant states of the $a_1^2(2)e^2$ configuration are

$$|\sigma_2\bar{\sigma}_2\sigma_3\bar{\sigma}_4\rangle = \frac{1}{\sqrt{2}}[^1E(0,y) + {}^3A_2(0)], \tag{2a}$$

$$|\sigma_2\bar{\sigma}_2\sigma_3\bar{\sigma}_3\rangle = \frac{1}{\sqrt{2}}[^1E(0,x) + {}^1A_1(0)], \tag{2b}$$

where $^1E(0,\lambda)$ is the multideterminant wave function of the singlet E state of $M_S=0$ at λ row ($\lambda=x$ or y) in Table I. The singlet single-Slater-determinant state of the $a_1^1(2)e^3$ configuration is

$$|\bar{\sigma}_2\sigma_3\sigma_4\bar{\sigma}_4\rangle = \frac{1}{\sqrt{2}}[^3E(0,x) + {}^1E(0,x)]. \tag{3}$$

In summary, the following many-body states must be considered: $^3A_2$, $^1A_1$, ^1E, ^3E, ^1E, and $^1A_1$. The two triplet states are orthogonal to each other, while the two $^1A_1$ and the two ^1E states theoretically can be mixed with each other. This will be discussed below. Our computational method described in the next section cannot take the spin-orbit and spin-spin interaction into account. From the energetic point of view those effects are marginal (within few meV), but they could have important consequences on the possible optical transitions and the spin state of the NV center.[23]

III. COMPUTATIONAL METHOD

We use density functional theory with the local spin density approximation (DFT-LSDA) of Ceperley-Alder,[36] as parametrized by Perdew and Zunger.[37] We employed three different codes and somewhat different methodologies to carry out the calculations. The geometry of the defect was optimized with the VASP code[38,39] and the SIESTA code.[40] The latter utilizes numerical atomic orbitals with Troullier–Martins pseudopotentials.[41] We applied the high level double-ζ plus polarization functions for both carbon and nitrogen atoms. In the SIESTA calculations, no symmetry restriction was applied. The linear combination of atomic orbitals analysis of the defect states is straightforward in this methodology through the wave function coefficients that are directly obtained from the SIESTA calculations. In the VASP calculations, we use a plane wave basis set with a cutoff of 420 eV($\approx$30 Ry), which is adequate for well converged calculations using projected augmented wave (PAW) pseudopotentials for the C and N atoms.[42,43] In the VASP calculations, we applied the C_{3v} symmetry, and the energy of the ground state, as well as that of the excited states are calculated by setting the appropriate occupation of the defect states in the gap. In the geometry optimization calculations, all the atoms were allowed to relax until the magnitude of the calculated forces was smaller than 0.01 eV/Å. The use of two different methods (VASP and SIESTA) with very different basis sets is a stringent check of the reliability of the results. SIESTA is well suited for the calculation of the coefficient α in Eq. (1). Coefficients of the atomic orbitals, VASP, on the other hand, have variational convergence and are suitable for obtaining the ground state properties (such as the spin density) because the convergence of the basis set size can be easily verified. All together, these methods add to the level of confidence for the accurate representation of the physics of the system

TABLE II. The calculated principal values of the hyperfine tensor (columns 3–5) compared to the known experimental data (columns 6–8) in megahertz. The average of the three principal values yields the Fermi-contact term. The difference between the principal values and the Fermi-contact term gives the dipole-dipole term. Only atoms with a signal larger than 2 MHz are shown. The symmetrically equivalent number of C atoms is shown in the first column and their distance in angstroms from the vacant site in the second column. The experimental data on ^{14}N is taken from Refs. 17 and 49. Experimental data on ^{13}C atoms were taken from Ref. 49. EPR studies can directly measure only the absolute value of the hyperfine constants, which is indicated by adding a $\pm$sign to experimental values. The calculated hyperfine tensors can be used for comparison with spin-echo measurements (see text). The modulation frequency $\omega^{(X)}$ in Eq. (7) is also given in megahertz. The experimental values $\omega^{(X)}_{expt}$ (in megahertz) are shown in parentheses, whenever the accuracy of the calculation does not allow for an unambiguous identification of the origin of $\omega^{(X)}_{expt}$.

Atom	R_{vac}	A_{11}	A_{22}	A_{33}	A_{11}^{expt}	A_{22}^{expt}	A_{33}^{expt}	$\omega^{(X)}$	$\omega^{(X)}_{expt}$
^{14}N	1.68	−1.7	−1.7	−1.7	±2.1	±2.1	±2.3	1.7	
3C	1.61	109.5	110.2	185.4	±123	±123	±205	158.5	
6C	2.47	−4.8	−3.7	−1.5				3.2	
3C	2.49	−7.4	−7.3	−5.8				7.3	9
6C	2.90	2.8	3.3	4.6				3.3	
3C	2.92	1.4	2.4	2.9				1.6	
3C	2.93	3.4	4.7	4.9				4.0	(4)
6C	3.85	13.5	14.2	19.4				17.5	
3C	3.86	12.8	12.8	18.0	±15.0	±15.0	±15.0	16.2	14
6C	4.99	2.6	2.7	3.8				2.8	
3C	5.00	1.5	1.5	2.2				1.5	

under study. We have also compared the results that are separately obtained by these two schemes and found that they are in very good agreement. The hyperfine tensor of the NV center was calculated by the CPPAW code.[44] In the CPPAW calculations, we used a 30 Ry cutoff for the plane wave basis with PAW projectors, a methodology virtually equivalent with the one used in the VASP calculations.

Convergence of calculated defect properties with supercell size is an important consideration. For this reason, we have chosen to model the NV center by using a large 512-atom simple cubic supercell. The lattice constant of the supercell ($\approx$14.2 Å) is four times larger than the lattice constant of the conventional cubic cell of diamond (a_0 =3.54 Å). We used the Γ-point sampling in the Brillouin zone, which corresponds to sampling finer than a $6\times6\times6$ grid of the primitive lattice; this provides a well converged charge density. It is also advantageous to restrict the calculations to the Γ point in order to keep the degeneracy of the e defect states, which may split in a general k-point sampling of the Brillouin zone. We checked that the geometry was practically identical (to within 0.01 Å) going from a 216-atom fcc supercell to the 512-atom simple cubic supercell. We will show that the calculated spin density, for instance, decays at much shorter distance than the lattice constant of the supercell. Thus, the 512-atom supercell is adequate to represent the isolated NV defect in a realistic manner.

We calculated the hyperfine tensor of the defect with the optimized geometry obtained by the VASP code. In the calculation of the hyperfine tensor, the relativistic effects are taken into account.[45] The hyperfine tensor of nucleus I consists of the Fermi-contact term (first parentheses in the following equation) and the dipole-dipole term (second parentheses),

$$A_{ij}^{(I)} = \frac{1}{2S}\int d^3r n_s(\mathbf{r})\gamma_I\gamma_e\hbar^2\left[\left(\frac{8\pi}{3}\delta(r)\right)+\left(\frac{3x_ix_j}{r^5}-\frac{\delta_{ij}}{r^3}\right)\right], \tag{4}$$

where $n_s(\mathbf{r})$ is the spin density of the spin state S, γ_I is the nuclear Bohr magneton of nucleus I, and γ_e is the electron Bohr magneton. The Fermi-contact term is proportional to the spin density localized at the place of the nucleus, which is dominant compared to the dipole-dipole term. We calculate the hyperfine tensor and diagonalize it in order to obtain its principal values, also called *hyperfine constants*. These hyperfine constants can be directly compared to experimental data. The Fermi-contact and the dipole-dipole terms are simply derived from the trace of the hyperfine constants ($\mathrm{Tr}[A_{ij}]/3$) and the deviation from the trace ($[A_{33}-\mathrm{Tr}[A_{ij}]/3)]/2$). If the dipole-dipole term is nonzero, then the signal is anisotropic. The ratio of the Fermi-contact and dipole-dipole terms characterizes the shape of the spin density.

The contribution of s-like wave functions to the charge density has a large effect on the Fermi-contact term, but, negligible effect on the dipole-dipole term since the s-like wave function has a maximum at the positions of the nuclei and is an even function. In contrast to this, the contribution of p-like wave functions to the charge density has a negligible effect on the Fermi-contact term, but a large effect on the dipole-dipole term since the p-like wave function has a node at the place of nuclei and is an odd function. Typically, the contribution of the dipole-dipole term is significant for the spin density built from well-localized dangling bonds, that is, the sp^3 hybrid orbitals (see Table II). We note that the pseudopotential methodology produces artificially smooth

wave functions close to the nuclei; therefore, only the all-electron PAW methodology can provide reliable hyperfine tensors. In the PAW methodology the calculation of the hyperfine tensor is somewhat more subtle than that shown in Eq. (4) and the dipole-dipole term is not fully calculated (see the appropriate note in Ref. 45) which causes about 0.3 MHz inaccuracy in the calculated dipole-dipole term in our case. This error could be important to take into account for hyperfine tensors with small matrix elements (<3 MHz). The total spin density, $n_s(\mathbf{r})$, can be defined as

$$n_s(\mathbf{r}) = n_{\text{up}}(\mathbf{r}) - n_{\text{down}}(\mathbf{r}),$$

where $n_{\text{up}}(\mathbf{r})$ and $n_{\text{down}}(\mathbf{r})$ are the spin densities built from spin-up and spin-down electrons, respectively. By taking the $M_S=1$ state of the $^3A_2$ state into account, as shown in Fig. 2, we expect that $n_s(\mathbf{r})$ will be positive. We will show that this is not true for the entire space around the defect.

IV. ATOMIC AND ELECTRONIC STRUCTURE OF THE NITROGEN-VACANCY DEFECT

A. Geometry and electronic levels

We begin with a discussion of the geometry optimization of the negatively charged NV center obtained from the SIESTA calculations using spin polarization and no symmetry restrictions. The defect automatically finds the $S=1$ state and maintains the C_{3v} symmetry of the original unrelaxed structure. The calculated one-electron defect levels are shown in Fig. 2. The first neighbor C and N atoms clearly relaxed outward from the vacancy. The calculated distances from the vacant site are 1.63 and 1.69 Å for the C atoms and the N atom, respectively. That is, the N atom relaxes more than the C atoms. We note that the C-vacancy distances are the same within 0.0002 Å without any symmetry constraints after geometry optimization. The N-C bond lengths are 1.46 Å, while the bond lengths of C radicals are 1.50 Å, which is not far from 1.44 and 1.45 Å, respectively, obtained in an LDA molecular cluster calculation.[34] The localized basis sets can have problems in the description of vacancy-like defects. Our VASP calculation, which employs a plane wave basis set, basically shows the same geometry after optimization: the calculated distances from the vacant site are 1.62 and 1.68 Å for the C atoms and the N atom, respectively. Thus, we conclude that the double-ζ plus polarization basis provides results very close to those of the converged plane wave basis set.

In an earlier work by Łuszczek *et al.*,[22] a plane wave basis set with pseudopotentials was employed in a 64-atom cubic supercell using $2\times2\times2$ Monkhorst-Pack Brillouin zone sampling[46] to investigate the NV defect in diamond. In that work, only the nearest neighbor atoms to the vacant site were allowed to relax without symmetry restrictions and a geometry close to C_{3v} symmetry was obtained; the largest deviation in the C-vacancy distances was about 0.001 Å. The calculated distances from the vacancy were 1.67 and 1.66 Å for the C atoms and the N atom, respectively, which shows the opposite trend from what we find both in the SIESTA and in the VASP calculations in the larger unit cell. Most probably the difference is due to the insufficient relaxation condition restricted only to the first neighbor atoms around the vacant site. We plot the wave functions of the defect states obtained by the LSDA calculations in Fig. 3.

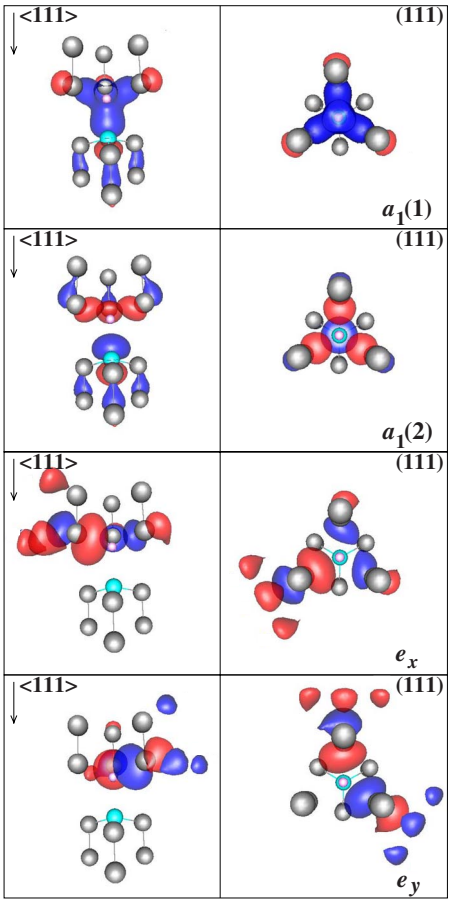

FIG. 3. (Color online) Isosurfaces of the calculated wave functions of the $a_1(1)$, $a_1(2)$, e_x, e_y defect states, shown in side (left) and top (right) views relative to the ⟨111⟩ axis. Blue (red) isosurfaces correspond to negative (positive) values of the wave function. The small pink circle represents the position of the vacant site, while the gray and cyan balls show the C and N atoms, respectively. We show the atoms up to the second neighbor from the vacant site. Results are from the SIESTA calculations.

The group theory analysis based on the single-particle picture describes very well the defect states. Naturally, the defect states are not strictly localized on the first neighbor atoms of the vacancy, but the largest portion of the wave functions can be indeed found there. The SIESTA calculation gives $\alpha\approx0.7$ for the parameter that appears in Eq. (1). This means that the N orbital is mostly localized on the $a_1(2):\phi_2$ defect level and has no amplitude on the e levels. Therefore, the nitrogen atom is only very weakly spin polarized in the $^3A_2$ state, while it is strongly spin polarized in the ^3E state [when one electron is excited from the $a_1(2)$ to level to the e level]. This is clearly shown in Fig. 4. It is apparent, from this figure, that the N atom is only weakly polarized (small negative spin density) in the $^3A_2$ state, while it is strongly polarized in the ^3E state comparable to the C ligands (large positive spin density). The spin density is always highly lo-

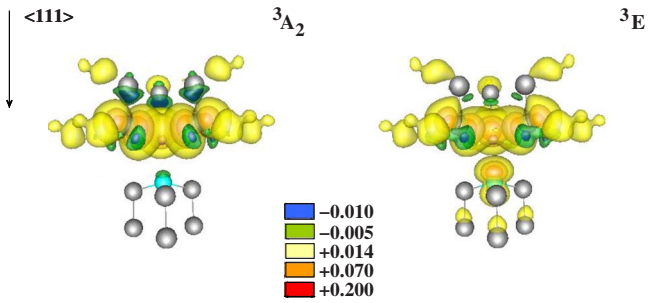

FIG. 4. (Color online) Calculated spin density isosurfaces in the $M_S=1$ state for the $^3A_2$ (left) and the ^3E state (right). The vacant site is depicted by a small pink sphere at the center of each plot. Results are from the VASP calculations.

calized on the three C atoms around the vacant site (orange lobes in the figure).

We also checked the situation when we optimized the geometry with the condition $S=0$. We already showed that the $|\sigma_2\bar{\sigma}_2\sigma_3\bar{\sigma}_3\rangle$ state is not an eigenstate with C_{3v} symmetry. In addition, this state is a Jahn-Teller unstable system. Indeed, the defect reconstructs to C_{1h} symmetry to remove the degenerate e level. However, this configuration is about 0.3 eV higher in energy than the $^3A_2$ state with C_{3v} symmetry.

B. Energy sequence of multiplets

From the structural analysis, we conclude that the dangling bonds around the vacancy do not form long bonds which could be the driving force of the reconstruction. Instead, the atoms relax outward from the vacancy and retain the strongly localized dangling bonds pointing to the vacant site which maintains the C_{3v} symmetry. Since the degenerate e defect level is only partially occupied, this is a typical situation where configurational interaction plays a crucial role. As shown above, most of the singlet eigenstates can be described only by multideterminant wave functions in C_{3v} symmetry. The optical transition takes place between the triplet states. We already showed the results on the $^3A_2$ state. In the VASP calculation, it is possible to set the occupation of one-electron states. The ^3E state can be achieved by setting zero occupation for the spin-down ϕ_2 level and full occupation of ϕ_3 spin-up and spin-down levels. The energy of the ^3E state can be calculated in the fixed geometry of the $^3A_2$ state, which yields the vertical ionization energy. Upon the excitation of the electron the nuclei can relax to find the minimum energy in the new configuration space. This relaxation can take place with the help of phonons around the defect. The ZPL transition corresponds to that energy where phonons do not participate between the energy minima of the two configurations, as shown in Fig. 5.

The calculated vertical ionization energy is 1.91 eV within LSDA. We found that the NV defect significantly relaxes due to this internal ionization. The C-vacancy distance is 1.67 Å, while the N-vacancy distance is 1.61 Å in the ^3E state. This shows the opposite trend than what was found in the $^3A_2$ state. This may be understood as follows: the N atom is strongly spin polarized in the ^3E state compared to $^3A_2$

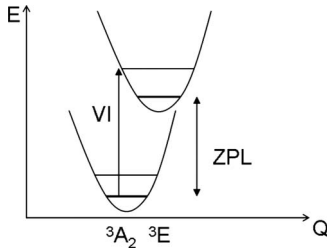

FIG. 5. Energetics of photoluminescence absorption: VI is the vertical ionization energy, ZPL is the zero-phonon line transition, E is the total energy, and Q is the configuration coordinate.

state, while the C ligands will be somewhat less spin polarized, which induces different charge transfers between the atoms in the ^3E state, and leads to a different geometry. The calculated relaxation energy (the Franck-Condon shift) is 0.2 eV. From this, we find a ZPL energy of 1.71 eV, which can be tentatively compared to the experimental value of 1.945 eV.[24,25] We note that a similar value (1.77 eV) was found by the LSDA molecular cluster calculation.[34] The LSDA excitation energy and the experimental transition energy are remarkably close to each other. This shows that the self-interaction error of LSDA for these defect levels does not differ too much, which is not unexpected since both of the defect states are basically valence band derived (from sp^3-like hybrid orbitals). Nevertheless, the calculated Franck-Condon shift, which is the relaxation energy defined as the energy difference between the vertical ionization energy and the ZPL energy, should be even more accurate than the calculated internal ionization energy. Indeed, the PL spectrum shows a broad phonon spectrum even at low temperature, and the intensity of the ZPL line is relatively small compared to the phonon side bands, which indicates a large Franck-Condon shift.

In addition to the triplet states it is worthwhile to calculate the energies of the singlet states because they play a significant role in the emission process, but these states have not yet been directly measured in experiments (see Ref. 23 and references therein). LSDA is not a suitable methodology to accurately calculate these energies. Beside the self-interaction error (which is relatively small for these defect levels as discussed above), LSDA gives the charge density of the interacting electrons, which is expressed in terms of the noninteracting Kohn-Sham particles. In DFT-LSDA, the wave functions are implicitly assumed to be single Slater determinants and hence they cannot accurately describe the singlet states, which are multideterminant states. Thus, the usual DFT-LSDA calculation cannot represent most of the singlet eigenstates of the NV center. This can be corrected by using a perturbation theory within DFT-LSDA, as explained by Lannoo *et al.*[47] Here, though, we adopt a more approximate method,[48] which was already applied for some states of this defect in Ref. 34. Our goal is to give approximate energies of the singlet eigenstates in order to predict their *sequence*, and we do not attempt to provide energies directly comparable to the experiments.

One of the $^1A_1$ states can be described by a single Slater-determinant [when the $a_1(2)$ level is totally empty and the e level is fully occupied]. This state can be calculated with

geometry optimization by LSDA as was explained for the ^3E state. We therefore concentrate on the remaining $^1A_1$ and two ^1E states. While the $|\sigma_2\bar{\sigma}_2\sigma_3\bar{\sigma}_3\rangle$, $|\sigma_2\bar{\sigma}_2\sigma_3\bar{\sigma}_4\rangle$, and $|\sigma_2\sigma_3\bar{\sigma}_3\bar{\sigma}_4\rangle$ single Slater determinants are not eigenstates, they can be expressed as the linear combination of different eigenstates, as shown in Eqs. (2a), (2b), and (3). von Barth[48] showed that the LSDA total energy ($\mathcal{E}$) of the mixed state can be expressed as the appropriate sum of the energy of the eigenstates, which yields the following equations:

$$\mathcal{E}[|\sigma_2\bar{\sigma}_2\sigma_3\bar{\sigma}_4\rangle] = \frac{1}{2}(\mathcal{E}[^1E] + \mathcal{E}[^3A_2]), \tag{5a}$$

$$\mathcal{E}[|\sigma_2\bar{\sigma}_2\sigma_3\bar{\sigma}_3\rangle] = \frac{1}{2}(\mathcal{E}[^1E] + \mathcal{E}[^1A_1]), \tag{5b}$$

$$\mathcal{E}[|\bar{\sigma}_2\sigma_3\sigma_4\bar{\sigma}_4\rangle] = \frac{1}{2}(\mathcal{E}[^3E] + \mathcal{E}'[^1E]). \tag{5c}$$

The ^1E state appearing in Eq. (5a) and (5b) belongs to the $a_1^2(2)e^2$ configuration, while the ^1E in Eq. (5c) belongs to the $a_1^1(2)e^3$ configuration (see Table I); hence, the corresponding energies are different and are denoted by different symbols, $\mathcal{E}[^1E]$ and $\mathcal{E}'[^1E]$, respectively. In Eqs. (5a) and (5c), we assume that the energy of the triplet states with $M_S=0$ and $M_S=1$ is the same. This is a very good approximation since, for instance, the experimentally measured splitting is about 2.88 GHz (few μeV) for the ground state due to spin-spin interaction,[16] while the spin-orbit splitting for the ^3E state is expected to be within few meV, which is far beyond the accuracy of LSDA calculations. The energy of the mixed states on the left hand side of Eqs. (5a)–(5c) can be directly calculated by LSDA. Since $\mathcal{E}[^3A_2]$ is known, $\mathcal{E}[^1E]$ can be determined from Eq. (5a). Similarly, $\mathcal{E}[^1E]$ can be determined from Eq. (5c). By combining Eqs. (5a) and (5b), we arrive at

$$\mathcal{E}[^1A_1] = 2(\mathcal{E}[|\sigma_2\bar{\sigma}_2\sigma_3\bar{\sigma}_3\rangle] - \mathcal{E}[|\sigma_2\bar{\sigma}_2\sigma_3\bar{\sigma}_4\rangle]) + \mathcal{E}[^3A_2]). \tag{6}$$

Thus, the $^1A_1$ state can also be determined.

von Barth[48] successfully applied this approach to calculate the energy of atoms in different states. Formally, this method can also be applied to the NV defect in diamond, but attention must be paid to relaxation effects. Generally, if the electron state changes, then it may imply also relaxation of the ionic positions, as was the case for the ^3E state discussed earlier. Relaxation effects cannot be taken into account with this methodology since only the energy of the mixed states can be directly calculated with LSDA, and the relaxation of the mixed state is meaningless. In other words, the geometry must be fixed in these calculations. The occupation of the e state varies in the case of the $^1A_1$ and ^1E states of the $a_1^2(2)e^2$ configuration. We assume that the geometry would involve negligible change from the geometry of the $^3A_2$ state, which belongs also to the $a_1^2(2)e^2$ configuration. Therefore, we fix the geometry obtained in the $^3A_2$ state when calculating the $^1A_1$ and ^1E states of the $a_1^2(2)e^2$ configuration. By using the same argument, we fix the geometry obtained for the ^3E state in the calculation of the ^1E state of the $a_1^1(2)e^3$ configuration. With these, we find the following energy sequence of the multiplets:

$$\mathcal{E}[^3A_2] \xrightarrow{\approx 0.0\ \text{eV}} \mathcal{E}[^1A_1] \xrightarrow{\approx 0.9\ \text{eV}} \mathcal{E}[^1E] \xrightarrow{\approx 0.8\ \text{eV}} \mathcal{E}[^3E] \xrightarrow{\approx 0.5\ \text{eV}} \mathcal{E}[^1E] \xrightarrow{\approx 1.3\ \text{eV}} \mathcal{E}[^1A_1].$$

That is, the deeper $^1A_1$ state is close in energy to the $^3A_2$ state, and the deeper ^1E state is below the ^3E state. The energy differences between the triplet states were already discussed.

We focus next on the singlet states. Within our approximate methodology the $^3A_2$ and $^1A_1$ states are almost degenerate. Close inspection of Eq. (6) reveals that the energy sequence of the $^3A_2$ and $^1A_1$ states depends on the energy difference of two singlet states: $(\mathcal{E}[|\sigma_2\bar{\sigma}_2\sigma_3\bar{\sigma}_3\rangle] - \mathcal{E}[|\sigma_2\bar{\sigma}_2\sigma_3\bar{\sigma}_4\rangle])$. We obtain almost zero for this energy difference. However, the LSDA self-interaction error may be larger for the $|\sigma_2\bar{\sigma}_2\sigma_3\bar{\sigma}_3\rangle$ state (where the exchange energy of σ_3 appears) than for the $|\sigma_2\bar{\sigma}_2\sigma_3\bar{\sigma}_4\rangle$ state (where the electrons occupy spatially orthogonal orbitals). This may raise the energy of the $\mathcal{E}[^1A_1]$ state. Nevertheless, this fact can be partially compensated by the relaxation effect of the $^1A_1$ state, which we are neglecting by necessity as explained before. An additional issue is the possible mixing with the higher $^1A_1$ state. We argue that the two $^1A_1$ states are not likely to mix because they are very far from each other in energy.

From the above analysis, we conclude that the $^1A_1$ state is indeed close in energy to the $^3A_2$ state. This may imply a very complicated fine structure of the states. The $^3A_2$ is the symmetry of the orbital wave function, and the $M_s=0$ and $M_s=\pm 1$ states are degenerate. However, if the spin-spin interaction is taken into account then the energy of the $M_s=\pm 1$ and the $M_s=0$ states will split. In the case of spin-spin interaction we have to take into account the symmetry of the spin function as well, which is E for the $M_S=\pm 1$ and A_2 for the $M_s=0$ state. The symmetry of the total wave function is the product of the orbital wave function (A_2) and the spin functions. Finally, one obtains $A_1=A_2\otimes A_2$ ($M_s=0$) and $E=A_2\otimes E$ ($M_s=\pm 1$). For more details, see Ref. 23 [specifically Fig. 1(a)]. The $^1A_1$ state becomes $A_1(M_S=0)$ (the spin state is not a good quantum number anymore, only its projection is). If the two $A_1(M_S=0)$ states are close in energy, then they may mix with each other. It is also important to notice that the energy of the deeper ^1E state falls between the energies of the triplet states. The relaxation effect may lower the energy of this state. In addition, the two ^1E states are not far from each other in energy, so the off-diagonal elements in the Hamiltonian may not be neglected. The mixing of the two ^1E states would further lower the energy of the deeper ^1E state and would raise the energy of the higher ^1E state. The final conclusion is that there are two singlet states between the triplet states, and the $^1A_1$ state is much closer in energy to the ground state than the ^1E state. The energies of the other two singlet states are certainly above that of the ^3E state.

The deeper singlet $^1A_1$ and ^1E states can play an important role in the emission process of the NV center. Experiments indicate that there should be a possibly long-living singlet state between the triplet states (see Ref. 23 and references therein). Usually, the singlet $^1A_1$ is considered in this process. However, our calculations indicate that there are two singlet states between the triplet states. Goss *et al.*[34] reported the sequence of $^3A_2$, ^1E, $^1A_1$, and ^3E states which is surprising in light of the previous discussion, as these states were obtained by LSDA molecular cluster calculations. Manson *et al.*[23] recently showed that if the ^1E state is above the $^1A_1$ state, the known properties of the emission can be consistently explained similar to the original singlet $^1A_1$ model, with the only difference being that the ^1E and $^1A_1$ states both contribute to the spin polarization process during the optical cycling and that the effect will be more efficient. Having the $^1A_1$ state higher in energy than the ^1E state would result in no change in spin orientation during optical cycling which is in contradiction with experiment.[23] From this point of view, our results that are obtained from approximate calculations are consistent with the PL experiments.

V. HYPERFINE CONSTANTS

As mentioned in the Introduction, the NV center in diamond is a promising candidate to realize qubit solid state devices operating at room temperature (Ref. 14 and references therein). The qubit is the nonzero (S=1) electron spin ground state which can interact with the neighbor ^{13}C isotopes possessing $I=1/2$ nuclear spin via hyperfine interaction. The natural abundance of the ^{13}C isotope is about 1.1%, so we can assume the same abundance in the diamond lattice. In conventional EPR measurements, the EPR absorption signal is detected on the *ensemble* of the defects in the diamond sample. The sample should be thick enough for absorption measurements and the concentration of the defects should be sufficiently high. Finally, a large number of defects is measured at the same time by EPR, so statistics can be applied to analyze the data. If the spin density is strongly localized on three *symmetrically equivalent* C ligands (see Fig. 4), then the probability of finding one ^{13}C atom among them is given by the binomial distribution and is about 3.2%. Finding two or three of them has negligible probability. Due to the $I=1/2$ nuclear spin, the hyperfine interaction splits into two lines with $I_z=1/2$ and $I_z=-1/2$ and therefore the intensity ratio between the main hyperfine line (involving no hyperfine interaction with ^{13}C atoms) and the hyperfine line associated with the C ligands will be roughly 1.5%. This makes the EPR measurement on ^{13}C hyperfine interaction a challenging task since the signal to noise ratio should be very good and the intensity of the EPR signal should be strong enough and stable to identify the satellite hyperfine lines due to ^{13}C isotopes.

The ^{13}C hyperfine interaction has been detected in EPR from two sets of three symmetrically equivalent C atoms by Loubser and van Wyk.[16,49] The larger hyperfine constants were associated with the C ligands of the NV center. In addition, the hyperfine interaction of the ^{14}N isotope was found in the NV center by EPR and ENDOR measurements.[16,17] To our knowledge, hyperfine interaction with other ^{13}C isotopes has not been directly measured by using EPR. We can estimate the localization of the charge density on the C and N atoms that are immediate neighbors of the vacant site from the linear combination of the atomic orbitals as they appear in the wave functions. He *et al.*[17] estimated that 72% and 0.2% of the charge density is localized on the three C ligands and the N atom, which leaves approximately 28% of the charge density to be spread in the lattice. Wrachtrup *et al.*[3] speculated that the spin density exponentially decays as a function of the distance from the vacant site. Since the hyperfine constants are roughly proportional to the spin density, as Eq. (4) indicates, these authors proposed that nine or more carbon nuclei should have a hyperfine value of 70 MHz in the second neighborhood, while the more distant carbon atoms should have a hyperfine constant smaller than 10 MHz. This proposal is not entirely consistent with the known EPR data since isotropic hyperfine splitting of 5.4 G (≈15 MHz) was measured from three ^{13}C isotopes,[49] whereas a value of 70 MHz hyperfine splitting should be measurable by EPR because it would not be obscured by the main EPR line.

In their theoretical treatment of the NV center, Łuszczek *et al.*[22] claimed that they can support the proposal of Wrachtrup *et al.*[3] based on their *ab initio* results. They optimized the geometry without symmetry constraints only for the first neighbor atoms of the vacancy in a 64-atom supercell. The adequacy of this restriction was already discussed above; with this restriction, while the C_{3v} symmetry is almost retained, the calculated Fermi-contact hyperfine interactions for the three C ligands deviate from each other more than 10% (see Table II in Ref. 22). This suggests that the spin density was not adequately converged in that calculation since the small deviation in the geometry from the C_{3v} symmetry could not imply such a large discrepancy in the calculated hyperfine field. These authors also calculated the Fermi-contact hyperfine interaction for the C atoms situated about 2.5 Å away from the vacant site. The reported numbers were about an order of magnitude smaller than for the C ligands, which led to the conclusion that the spin density and the corresponding hyperfine constants should decay fast for other C atoms farther from the vacant site.

In addition to the problem of the inconsistent values of the hyperfine interaction for the three C ligands, several other issues related to the results of Ref. 22 must be mentioned:

(i) These authors have actually reported the hyperfine *field* and not the hyperfine *constant*. However, the conversion from the hyperfine field, which is the magnetization density on the atom and it is a number directly obtained from the computation, to the hyperfine constant is not unique; therefore, it is very difficult to compare the calculated values to the experimental data.

(ii) Only the Fermi-contact term was calculated, while the dipole-dipole term can be also significant; this is known to be the case for the C ligands from experimental measurements.[16,49]

(iii) The hyperfine interaction with distant C atoms could be very important for qubit applications based on this defect, so the hyperfine tensor must be calculated at larger distances from the vacancy.

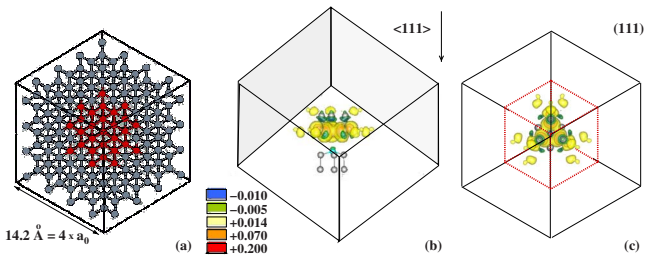

FIG. 6. (Color online) (a) The 512-atom cubic supercell with all C atoms shown (atoms within a 64-atom supercell are shown in red). The supercell size in angstroms and in units of the conventional cubic cell lattice constant a_0 is indicated on the side of the cube. (b) Perspective view of the calculated spin density isosurfaces in the $M_S=1$ state. Only atoms up to the second nearest neighbor of the vacant site are shown. (c) View along the (111) direction indicating the C_{3v} symmetry of the spin density, which is given in colored contours. The black lines denote the size of the 512-atom supercell, while the red dotted ones show the boundaries of the 64-atom supercell.

Based on these arguments, we believe that the nature of the spin density and the corresponding hyperfine interaction with the ^{13}C isotopes has not yet been explored in detail despite its high importance.

Toward establishing the nature of this interaction, we show first the calculated spin density in our 512-atom supercell in Fig. 6. As expected, the spin density is highly localized around the three C ligands nearest to the vacant site (orange lobes in the figure), within a radius of $1\times a_0$ from this site. The spin density practically vanishes at distances $>2\times a_0$ from the vacant site. Below the three C atoms (see Fig. 6), there is the N atom with a small *negative* spin density. Some C atoms farther from the vacant site also have negative spin density. The spin density mostly extends on a plane perpendicular to the (111) direction and no measurable spin density can be found below the N atom. On the N atom, the spin density is negative. It was shown earlier that the spin density mostly comes from the spin-polarized e level localized on the C dangling bonds, and due to symmetry reasons, orbitals related to the N do not appear in the e level. The tiny negative charge density on the N atom can be explained by the polarization of its core states: since the nuclear Bohr magneton of the N atom is positive, the Fermi-contact term will be negative (see Table II). Overall, the spin density is spread on a plane perpendicular to the (111) direction. There are some C atoms which have significant negative spin density which results in a negative Fermi-contact term. No measurable hyperfine interaction (spin density) can be found for the C atoms below the N atom. Loubser and van Wyk[49] speculated that the 15 MHz ^{13}C isotropic hyperfine splitting comes from the three C atoms bonded to the N atom. Our calculation negates this possibility.

Table II shows that there is a local maximum of the spin density at $R_{\rm vac}\approx 3.9$ and 5.0 Å, where $R_{\rm vac}$ is the distance from the vacant site. At $R_{\rm vac}>6.3$ Å, the calculated hyperfine constants are below 1 MHz, which means that the spin density vanishes at $R_{\rm vac}\approx 2\times a_0$. Apparently, the 64-atom supercell is too small to capture these properties due to the artificial overlap of the spin density caused by the periodic boundary conditions. We also find that the charge density does not monotonically decay such as an exponential function, but oscillates with the distance from the vacant site and decays fast (see Fig. 7).

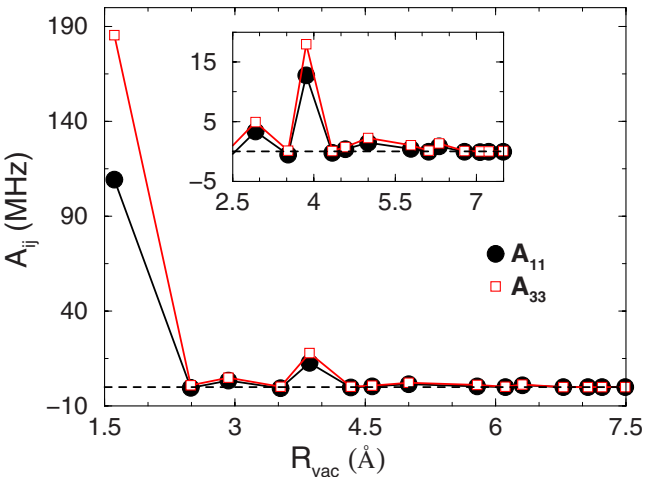

FIG. 7. (Color online) Variation of the principal values of the hyperfine tensors A_{11} and A_{33} as a function of the distance from the vacant site ($R_{\rm vac}$) for the set of three symmetrically equivalent C atoms (3C). In the inset, we show changes farther from the vacant site on a finer scale. The variation for the set of six symmetrically equivalent C atoms closely follows the one shown for 3C.

It is important to compare the calculated hyperfine values to the known experimental data in order to estimate the accuracy of our calculations. For that purpose, the hyperfine constant of the N atom is not the best choice because its value is very small and it is caused by only indirect spin-polarization effect. As mentioned above, there is an inherent inaccuracy in the calculated dipole-dipole term of about 0.3 MHz; therefore, it is reasonable to consider only values of the hyperfine constants that are significantly larger than this limit. Accordingly, we restrict the comparison to values that are higher than 2 MHz. By comparing the hyperfine constants of the C ligands, we estimate the inaccuracy for both the Fermi-contact term and the dipole-dipole term to be about 10%. This is usual for LSDA calculations.[18–21] The calculated ratio between the Fermi-contact term and the dipole-dipole term remarkably agrees well with experiment for the C ligands, i.e., 5.36 and 5.50, respectively. This shows that the shape of the spin density is very well described by LSDA. This ratio indicates that the p-functions dominate by about 90% in the dangling bonds, so those are more p-like orbitals than sp^3 hybrids. The reason is most likely the outward relaxation of the C atoms from the vacant site. The plotted wave functions indeed show a very strong p contribution of the e levels in Fig. 3, while the spherical s contribution is very small. The shape of the wave functions can be directly compared to the proposed wave functions in Eq. (1) from the group theory analysis of the defect diagram. Specifically, the $a_1(1)$ state is a combination of the p orbitals of all three carbon dangling bonds with that of nitrogen (all σ_i, $i=1,4$ in Fig. 1), with the same sign in the wave function, as shown by the blue isosurface that surrounds all these atoms. Similarly, the $a_1(2)$ state is formed again by the com-

bination of all first neighbors to the vacant site. In this case, the sign of the wave function localized on the carbon atoms is the opposite of that localized on the nitrogen atom, as indicated by the different colors of the isosurface in Fig. 3. On the other hand, the e_x and e_y states are formed only by the carbon dangling bonds. In the former, all three carbon dangling bonds are involved, as indicated by the red and blue isosurfaces around them, while in the latter, only two of them (σ_2 and σ_3 in Fig. 3) are involved in the bonding.

An additional 15 MHz ^{13}C hyperfine splitting was measured by Loubser *et al.*[49] by using EPR but the measured spectrum of the NV center was not shown in detail; therefore, we cannot comment on the accuracy of this measurement. Nevertheless, that work stated that the hyperfine splitting is isotropic, that is, the dipole-dipole term is negligible, and the relative intensity of the hyperfine satellite line and the main EPR line indicates the involvement of three symmetrically equivalent C atoms.[49] The likely candidate for this signal is found at the third neighbors of the vacant site at R_{vac}=3.86 Å. The spin density of these atoms is shown as yellow lobes above the small green lobes at the highest position on the side view in Fig. 6. The calculated anisotropy of this hyperfine interaction is about 3–4 MHz. If the uncertainty in the measurement is in this range due to line broadening, then the signal could be detected as nearly isotropic. However, our calculations reveal that six additional C atoms have similar hyperfine splitting at the third neighbor distance of R_{vac}=3.85 Å, corresponding to the six yellow lobes laterally spread farthest from the vacant site, which is most obvious from the view along the (111) direction in Fig. 6. This means that the hyperfine splitting due to these six C atoms would have to be simultaneously detected with the other three ones. Since the difference in the hyperfine splitting of these two sets of atoms is small, the six-atom set could obscure the signal of the three-atom set showing an effective relative intensity associated with six symmetrically equivalent C atoms. We suggest that this part of the spectrum should be experimentally reinvestigated in detail. The hyperfine splitting of 7–8 MHz from the ^{13}C atom may be also detectable by EPR, while the other signals may be too small and hence obscured by the main hyperfine lines.

Recently, individual NV centers have been detected by spin-echo measurements.[13,14] In particular, detailed results for six NV centers in diamond have been reported.[13] The spin-echo measurements have detected the coherent state of the electron spin coupled with a proximal ^{13}C nucleus. The coupling is due to hyperfine interaction between the electron spin and the nuclear spin of ^{13}C isotopes. The resulting spin-echo signals show a rapidly oscillating function enveloped by a more slowly oscillating function.[13] These authors proposed a theory to explain this signal, and they concluded that the fast modulation frequency is due to the effective magnetization density of the electron spin felt by the ^{13}C nucleus, which is the same as the hyperfine interaction. The modulation frequency can be well approximated as the norm of the hyperfine tensor projected to the symmetry axis, which leads to the following expression within our formulation of the problem:

$$\omega^{(\mathbf{X})} = |\hat{\mathbf{u}}_{[111]} \otimes \mathbf{A}_{\mathbf{ij}}^{(\mathbf{X})}|, \tag{7}$$

where $\hat{u}_{[111]}$ is the appropriate projection vector and $\mathbf{A}_{\mathbf{ij}}^{(\mathbf{X})}$ is the hyperfine tensor of nucleus X. Since we calculate the full $\mathbf{A}_{\mathbf{ij}}^{(\mathbf{X})}$ tensor [see Eq. (4)], the calculation of the modulation frequency is straightforward. Modulation frequencies have been reported for four single NV defects (see Fig. 4B of Ref. 13). A single modulation frequency was measured for each NV center at ≈2, ≈4, ≈9, and ≈14 MHz, respectively, so these particular NV centers had hyperfine interaction with one ^{13}C isotope in the lattice.[13] It would be useful to compare the hyperfine interaction measured by EPR and spin-echo techniques which can be an additional validation of the theory developed by Childress *et al.*[13] As was explained earlier, conventional EPR tools have limitations in detecting ^{13}C isotopes. A ^{13}C enriched sample would be useful to experimentally study this defect in more detail.

The largest ^{13}C hyperfine splitting corresponds to a modulation frequency that is too large to be detected by spin-echo measurements. However, an isotropic ^{13}C hyperfine splitting of 15 MHz has also been reported.[49] The isotropic signal means that the modulation frequency should also be about 15 MHz. This is very close to one of the measured modulation frequencies at ≈14 MHz.[13] From the calculated hyperfine tensors in Table II, this signal must originate from a C atom, which is a third neighbor of the vacant site at R_{vac} =3.86 Å. The calculated modulation frequency is ≈16 MHz, which is close to the measured one taking into account the limitations of our computational method. If one takes into account the accuracy in the calculation of the hyperfine constants, then the 6C at 3.85 could be excluded. The 9 MHz spin-echo signal can originate only from the atoms at R_{vac} =2.49 Å, and contributions from other neighbors can be safely excluded. In this way, the origin of the signal can be identified. The 4 MHz spin-echo signal can originate either from atoms at R_{vac}=2.90 Å or at R_{vac}=2.93 Å by taking into account computational limitations. In the first case, six symmetrically equivalent C atoms are involved, while in the second case, a set of three symmetrically equivalent C atoms are involved. It is difficult, if not impossible, to identify the origin of the 1 MHz spin-echo signal, which is beyond the accuracy of our calculations. Nevertheless, the calculations indicate that this signal could arise from at least 12 C atoms. Most of them are far from the vacant site but some are closer than the atoms that give rise to the ≈14 MHz signal, as is evident from Fig. 7.

The number of symmetrically equivalent atoms is also specific to the individual hyperfine constant and therefore to the modulation frequency. Because of the C_{3v} symmetry, sets of three or sets of six C atoms are equivalent with each other. The relative occurrence of the modulation frequencies measured by spin-echo experiments helps in identifying the equivalent atoms around the vacancy. Four samples represent a rather limited set of values for statistical analysis, so the relative occurrence of ^{13}C isotopes picked up by these measurements cannot be used for such analysis. A much larger number of NV samples is needed in the spin-echo measurements in order to use the relative occurrence of the ^{13}C iso-

tope signals for the identification of individual atoms in the diamond lattice.

VI. SUMMARY AND CONCLUSIONS

In this work, we have investigated the negatively charged nitrogen-vacancy center in diamond in detail by *ab initio* supercell calculations by using density functional theory methods. We showed that the energy sequence of multiplet states is $^3A_2$, $^1A_1$, ^1E, ^3E, ^1E, and $^1A_1$. This means that the singlet ^1E state enhances the spin polarization process during the optical cycling of the defect. The center has nonzero spin ground state. The full hyperfine tensor for a large number of atoms around the defect was calculated. The calculated hyperfine constants of the C ligands agree well with the experimental values detected by electron paramagnetic resonance tools. However, there is a controversy about the number of symmetrically equivalent carbon atoms of the second highest hyperfine interactions when these are compared to experiment. We propose that part of the electron paramagnetic resonance spectrum should be reinvestigated in detail in order to clarify this issue. Our calculations reveal that the spin density of the ground state is spread in the lattice, mostly on a plane perpendicular to the (111) direction defined by the positions of the N atom and the vacant site, and that it does not monotonically decay from the vacant site. As a consequence, only a certain number of ^{13}C isotopes can interact with the electron spin, which can be used as qubits for quantum computing. By using the limited number of measurements that have been recently published for single nitrogen-vacancy centers detected by spin-echo measurements, we were able to identify some individual atoms around the defect. Our results contribute to the understanding of the spin-echo signals of the defect, which is a crucial step toward realization of the qubit concept in this system. Additional spin-echo measurements in NV samples will help identify other individual ^{13}C atoms around the defect.

ACKNOWLEDGMENTS

We are thankful to Liang Jiang, Jeronimo Maze, and Mikhail Lukin for encouraging discussions. A.G. acknowledges support from the Eötvös Foundation of Hungary. M.F. acknowledges support by Harvard's Nanoscale Science and Engineering Center, funded by the National Science Foundation, Grant No. PHY-0117795.

[1] A. Gruber, A. Drabenstedt, C. Tietz, L. Fleury, J. Wrachtrup, and C. Borczyskowski, Science **276**, 2012 (1997).
[2] A. Drabenstedt, L. Fleury, C. Tietz, F. Jelezko, S. Kilin, A. Nizovtzev, and J. Wrachtrup, Phys. Rev. B **60**, 11503 (1999).
[3] J. Wrachtrup, S. Y. Kilin, and A. P. Nizotsev, Opt. Spectrosc. **91**, 429 (2001).
[4] F. Jelezko, I. Popa, A. Gruber, C. Tietz, J. Wrachtrup, A. Nizovtsev, and S. Kilin, Appl. Phys. Lett. **81**, 2160 (2002).
[5] F. Jelezko, T. Gaebel, I. Popa, A. Gruber, and J. Wrachtrup, Phys. Rev. Lett. **92**, 076401 (2004).
[6] F. Jelezko, T. Gaebel, I. Popa, M. Domhan, A. Gruber, and J. Wrachtrup, Phys. Rev. Lett. **93**, 130501 (2004).
[7] R. J. Epstein, F. Mendoza, Y. K. Kato, and D. D. Awschalom, Nat. Mater. **1**, 94 (2005).
[8] R. Hanson, F. M. Mendoza, R. J. Epstein, and D. D. Awschalom, Phys. Rev. Lett. **97**, 087601 (2006).
[9] R. Brouri, A. Beveratos, J.-P. Poizat, and P. Gragier, Opt. Lett. **25**, 1294 (2000).
[10] A. Beveratos, R. Brouri, T. Gacoin, J.-P. Poizat, and P. Grangier, Phys. Rev. A **64**, 061802(R) (2001).
[11] L. Childress, J. M. Taylor, A. S. Sørensen, and M. D. Lukin, Phys. Rev. Lett. **96**, 070504 (2006).
[12] L. Jiang, J. M. Taylor, A. S. Sørensen, and M. D. Lukin, Phys. Rev. A **76**, 062323 (2007).
[13] L. Childress, M. V. Gurudev Dutt, J. M. Taylor, A. S. Zibrov, F. Jelezko, J. Wrachtrup, P. R. Hemmer, and M. D. Lukin, Science **314**, 281 (2006).
[14] M. V. Gurudev Dutt, L. Childress, L. Jiang, E. Togan, J. Maze, F. Jelezko, A. S. Zibrov, P. R. Hemmer, and M. D. Lukin, Science **316**, 312 (2007).
[15] L. Jiang, M. V. Gurudev Dutt, E. Togan, L. Childress, P. Cappellaro, J. M. Taylor, and M. D. Lukin, Phys. Rev. Lett. **100**, 073001 (2008).
[16] J. H. N. Loubser and J. P. van Wyk, in *Diamond Research (London)* (Industrial Diamond Information Bureau, London, 1977), pp. 11–15.
[17] X.-F. He, N. B. Manson, and P. T. H. Fisk, Phys. Rev. B **47**, 8816 (1993).
[18] T. Umeda, Y. Ishitsuka, J. Isoya, N. T. Son, E. Janzén, N. Morishita, T. Ohshima, H. Itoh, and A. Gali, Phys. Rev. B **71**, 193202 (2005).
[19] T. Umeda, N. T. Son, J. Isoya, E. Janzén, T. Ohshima, N. Morishita, H. Itoh, A. Gali, and M. Bockstedte, Phys. Rev. Lett. **96**, 145501 (2006).
[20] N. T. Son, P. Carlsson, J. ul Hassan, E. Janzén, T. Umeda, J. Isoya, A. Gali, M. Bockstedte, N. Morishita, T. Ohshima, and H. Itoh, Phys. Rev. Lett. **96**, 055501 (2006).
[21] T. Umeda, J. Ishoya, T. Ohshima, N. Morishita, H. Itoh, and A. Gali, Phys. Rev. B **75**, 245202 (2007).
[22] M. Łuszczek, R. Lakowski, and P. Horodecki, Physica B **348**, 292 (2004).
[23] N. B. Manson, J. P. Harrison, and M. J. Sellars, Phys. Rev. B **74**, 104303 (2006).
[24] L. du Preez, Ph.D. thesis, University of Witwatersrand, 1965.
[25] G. Davies and M. F. Hamer, Proc. R. Soc. London, Ser. A **348**, 285 (1976).
[26] A. T. Collins, J. Phys. C **16**, 2177 (1983).
[27] R. Hanson, O. Gywat, and D. D. Awschalom, Phys. Rev. B **74**, 161203(R) (2006).
[28] D. A. Redman, S. Brown, R. H. Sands, and S. C. Rand, Phys. Rev. Lett. **67**, 3420 (1991).
[29] N. R. S. Reddy, N. B. Manson, and C. Wei, J. Lumin. **38**, 46 (1987).
[30] E. van Oort, N. B. Manson, and M. Glasbeek, J. Phys. C **21**,

4385 (1988).
[31] N. B. Manson, P. T. H. Fisk, and X.-F. He, Appl. Magn. Reson. **3**, 999 (1992).
[32] J. P. Goss, R. Jones, P. R. Briddon, G. Davies, A. T. Collins, A. Mainwood, J. A. van Wyk, J. M. Baker, M. E. Newton, A. M. Stoneham, and S. C. Lawson, Phys. Rev. B **56**, 16031 (1997).
[33] A. Lenef and S. C. Rand, Phys. Rev. B **56**, 16033 (1997).
[34] J. P. Goss, R. Jones, S. J. Breuer, P. R. Briddon, and S. Öberg, Phys. Rev. Lett. **77**, 3041 (1996).
[35] A. Lenef and S. C. Rand, Phys. Rev. B **53**, 13441 (1996).
[36] D. M. Ceperley and B. J. Alder, Phys. Rev. Lett. **45**, 566 (1980).
[37] J. P. Perdew and A. Zunger, Phys. Rev. B **23**, 5048 (1981).
[38] G. Kresse and J. Hafner, Phys. Rev. B **49**, 14251 (1994).
[39] G. Kresse and J. Furthmüller, Phys. Rev. B **54**, 11169 (1996).
[40] D. Sanchéz-Portal, P. Ordejón, E. Artacho, and J. M. Soler, Int. J. Quantum Chem. **65**, 543 (1997).
[41] N. Troullier and J. L. Martins, Phys. Rev. B **43**, 1993 (1991).
[42] P. E. Blöchl, Phys. Rev. B **50**, 17953 (1994).
[43] G. Kresse and D. Joubert, Phys. Rev. B **59**, 1758 (1999).
[44] P. E. Blöchl, C. J. Först, and J. Schimpl, Bull. Mater. Sci. **26**, s33 (2001).
[45] P. E. Blöchl, Phys. Rev. B **62**, 6158 (2000).
[46] H. J. Monkhorst and J. K. Pack, Phys. Rev. B **13**, 5188 (1976).
[47] M. Lannoo, G. A. Baraff, and M. Schlüter, Phys. Rev. B **24**, 943 (1981).
[48] U. von Barth, Phys. Rev. A **20**, 1693 (1979).
[49] J. H. N. Loubser and J. A. van Wyk, Rep. Prog. Phys. **41**, 1201 (1978).